PHYSICAL REVIEW A VOLUME 46, NUMBER 8 15 OCTOBER 1992

Secondary instabilities in electroconvection in nematic liquid crystals

Satoru Nasuno, Osamu Sasaki, and Shoichi Kai
Department of Electrical Engineering, Kyushu Institute of Technology, Tobata, Kitakyushu 804, Japan

Walter Zimmermann
Department of Electrical Engineering, Kyushu Institute of Technology, Tobata, Kitakyushu 804, Japan and Institut für Festkörperforschung, Theorie III, Forschungszentrum Jülich, 5170 Jülich, Federal Republic of Germany

(Received 13 November 1991; revised manuscript received 15 June 1992)

We report experimental results on the stability diagram of the normal-roll pattern in electroconvection in nematic liquid crystals. The stable wave-number bands of the normal rolls are determined for various frequencies of the applied voltage. We find that the mode destablizing the normal rolls is of the zigzag type at low frequencies of the applied voltage and at higher frequencies mainly of the skewed varicos type. The change of the destablizing mode of the normal rolls is closely related to the change of the transition scenarios to weak turbulence. With increasing amplitude of the external voltage, at low frequencies the normal rolls are followed by a zigzaglike pattern and at higher frequencies they are followed by a breathing pattern consisting of a two-dimensional lattice of defects. Both secondary patterns are therefore on a different route to weak turbulence to which they finally bifurcate at higher voltages.

PACS number(s): 47.20.Ky, 47.65.+a, 61.30.Gd

I. INTRODUCTION

The physics of pattern formation has attracted considerable attention in various fields recently. In particular, the conditions for the formation of various types of well-ordered spatiotemporal patterns, pattern selection, and the loss of coherence are of a wider interest [1]. For investigating such problems fluid dynamical systems as, for instance, Rayleigh-Bénard convection (RBC) [2] and electrohydrodynamic convection (EHC) in nematic liquid crystals [3–5] have been used extensively because of their richness of phenomena, their experimental handiness, and their theoretical first-principles accessibility. In both systems, one has a fluid layer that is bounded from the top and the bottom by horizontal plates and across the layer an external stress is applied, which is for RBC a temperature difference and for EHC an ac voltage. These and other fluid dynamical systems all have in common that above a well-defined critical value of the external stress there appears a well-organized structure such as stationary periodic convection rolls. There is, however, a striking contrast between RBC of simple fluid and EHC in their symmetry. In the former the pattern can appear essentially with arbitrary orientation at a threshold, whereas in the latter there is a preferred orientation. Hence they provide prominent examples of isotropic and anisotropic pattern-forming systems, respectively. When external stress is further increased, then well-organized structures lose their stability and more spatiotemporally complex structures appear. The transition to weak turbulence, where spatial coherence is destroyed, however a dominant length scale still survives [6], has particularly attracted much attention [7–9].

One general and prominant approach to this problem is to study the destabilizing mechanism of a periodic pattern. For RBC of isotropic fluids the stability of periodic rolls has been studied in detail, both theoretically and experimentally [2], and the results obtained there provide important insights for the understanding of the physical origin of the onset of weak turbulence [10,11]. On the other hand, for EHC only a few investigations on the determination of the stability of convection rolls are available [12–16], and several questions are left open. For instance, experiments performed so far in EHC imply that the transition scenario from the stationary periodic rolls [Williams rolls (WR's)] to weak turbulence [the so-called fluctuating Williams rolls (FWR's) [17]] cannot fit into a unique scheme. To our knowledge, there are at least three different transition scenarios for increasing values of applied voltage. In the first scenario [4,15,17], the WR undergoes a direct transition to a FWR. In the second [4,16], the WR first undergoes a transition to a zigzaglike roll structure (ZZ) at a well-defined threshold and then a transition from ZZ to a FWR takes place at a higher threshold. In the third transition [18], instead of a ZZ one has another stable ordered phase between the WR and the FWR, where the WR is modulated periodically in both longitudinal and transversal directions. These scenarios have been all observed in unsystematic experimentals. This situation calls for a more systematic investigation of the stability of Williams rolls as well as on the transition scenarios in this system.

In this paper we present experimental results on the stability of the stationary periodic rolls (WR's) in EHC. The WR investigated here is oriented with its axis normal to the unperturbed director orientation and hence called *normal rolls* to distinguish from the WR with its oblique axis *(oblique rolls)* [19]. In order to make systematic measurements of the stability of normal rolls, the present experiments were performed by controlling three relevant

parameters of this problem, the wave number k of normal rolls, and applied voltage V, and its frequency f. We found that three types of secondary instabilities can occur depending on these parameters, i.e., the Eckhaus, the zigzag, and the skewed varicose instability. The stability diagram hence consists of these instability boundaries and shows striking dependence in its nature on the controlling parameters. Furthermore, we show that the three scenarios for the transition from a WR to a FWR as mentioned above occur in one experimental sample, however, in different frequency ranges. The change of the transitions with f is closely related with change of the dominant destabilizing mechanism of the WR.

The paper is organized as follows. In Sec. II we describe briefly our experimental setup and the experimental procedure used for determining the stability of normal rolls. In Sec. III we present our experimental results on the stability of the normal rolls, together with that on the transition scenarios. Finally we conclude with a discussion of our results in Sec. IV.

II. EXPERIMENT

A. Experimental setup

The geometry of the liquid-crystal cell used in the present experiments is similar to that described in Ref. [20]. In order to achieve a uniform planar alignment of the director $\hat{\mathbf{n}}$ in the nematic liquid crystal, the surface of the electrodes of the cell was coated previously with polyvinyl alcohol and then rubbed in one direction. The rubbing direction we call the x direction and the coordinate perpendicular to the cell plane we call the z direction. The distance between the transparent electrodes at the top and at the bottom is fixed with the space $d=25$ μm by a Mylar film at the lateral boundaries of the cell. The horizontal dimensions of the cell are $l_x=20$ mm and $l_y=20$ mm, so that the aspect ratios of the cell are $\Gamma_x=\Gamma_y=800$ with $\Gamma\equiv l/d$.

The nematic liquid crystal used in the present experiments is *N*-*p*-methoxybenzylidene-*p*-butylaniline (MBBA) doped with 0.01 wt.% of tetra-*n*-butylammonium bromide, whose nematic-isotropic transition temperature is about 39 °C. The controlled doping of the nematic liquid crystal with a small amount of dissociating organic molecules allows us to adjust the electrical conductivity—which is essential for the electrohydrodynamic instability—at the required values for the experiment. The nematic liquid crystal was introduced into the cell under vacuum conditions by taking advantage of the capillary action and then the cell was finally sealed completely to avoid deterioration. The temperature of the cell was kept constant at 30.00±0.01 °C.

The ac electric field applied across the liquid-crystal layer was generated by the digital wave synthesizer system (Analogic Co. Ltd. Data-2020). The convection patterns were visualized under a microscope with polarized light. Visualized images were taken with a charge-coupled-device (CCD) camera and stored on video tape. Images were typically taken from the central 0.1% of the cell area. The recorded images were analyzed by use of a

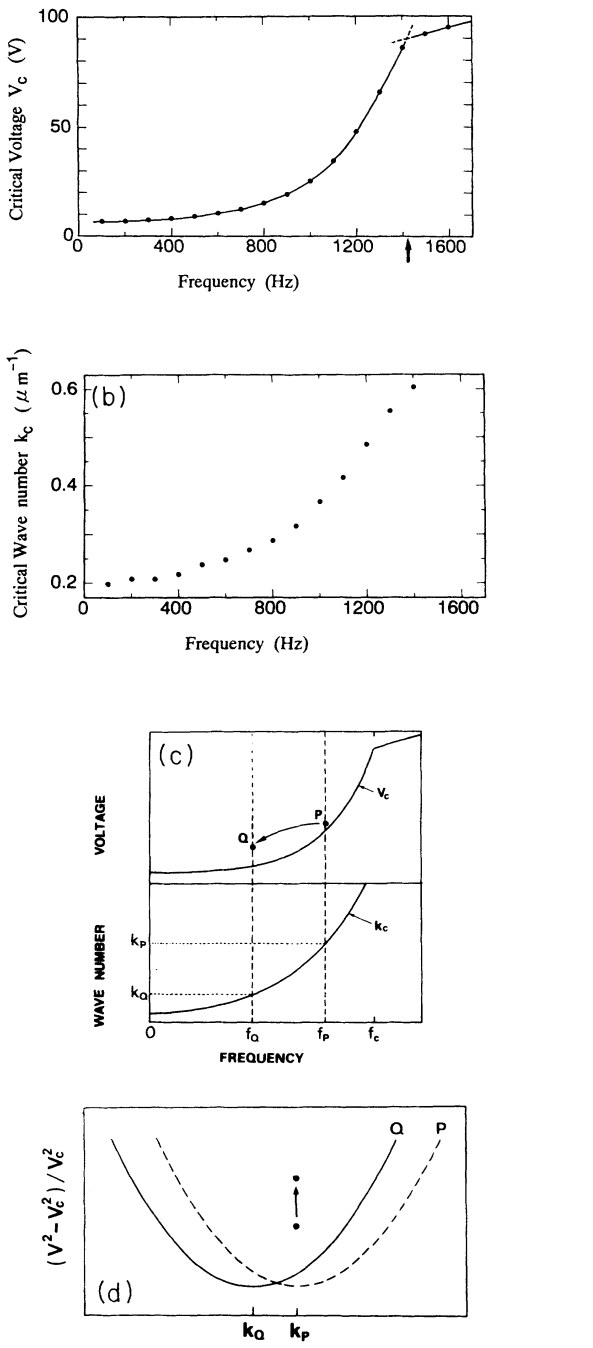

FIG. 1. (a) The critical voltage V_c for the onset of convection and (b) the critical wave number k_c as a function of the frequency of the external applied voltage. At the onset of convection we observe normal-oriented rolls in the whole conduction regime (below the cutoff frequency f_c which is indicated by the arrow). (c) and (d) A sketch of the voltage-frequency jump procedure is given. At f_P the convection-roll pattern occurring at threshold has the wave number k_P [(d) minimum of curve P]. After the voltage-frequency jump (V_Q,f_Q) the wave number is unchanged; however the position of the neutral curve ($P\rightarrow Q$) is changed and therefore so is the location of k_P with respect to the neutral curve. This procedure enables the preparation of convection rolls at well-defined wave-number voltage pairs (V,k).

digital image processor system with 512×512 pixels spatial resolution and eight-bit gray-scale resolution.

To give a fingerprint of our system, we present as a function of frequency f of the applied voltage in Fig. 1 the threshold voltage $V_c(f)$ and the critical wave number $k_c(f)$ of the roll pattern at the onset of convection. The cutoff frequency f_c of the sample is at 1400 Hz. Below the cutoff frequency f_c, we always get the normal rolls at the onset of convection, whose axis is normal to the x direction. In the present study, the voltage and the wave number is measured in normalized units $\epsilon=[V^2-V_c^2(f)]/V_c^2(f)$ and $q=k/k_c(f)$, respectively.

B. Experimental procedure

A detailed quantitative measurement on the stability of normal rolls requires the control on the wave number of rolls as well as the voltage and the frequency of the external field. This can be done efficiently by utilizing the frequency dependence of the critical wave number k_c [21] (see Fig. 1). The experimental procedure to investigate the stability of normal rolls with a given wave number k_P at a chosen frequency f_Q and at a chosen voltage V_Q is as follows.

(i) First, we prepare normal rolls with a given wave number k_P by setting the frequency f so that $k_c(f)=k_P$ and then increasing the voltage V slightly beyond the onset of convection.

(ii) Then both the frequency and the amplitude of the applied voltage are changed simultaneously to the aimed values f_Q and V_Q. In this manner we can prepare the normal rolls with a desired wave number k_P at a chosen frequency f_Q and a chosen voltage V_Q and test its stability. Repeating this procedure for many different values of k_P, f_Q, V_Q we can determine the stability range of normal rolls as a function of k, V, and f. It is helpful to consider this procedure in terms of the position of the neutral stability curve $\epsilon_0(k,f)$ for the onset of convection. If the voltage-frequency jump is made in the frequency from f_P to f_Q but with keeping ϵ fixed, one will have some relative shift of the neutral curve along the k axis with respect to k_P as sketched in Fig. 1(d). In a more general case, the voltage-frequency jump can give also an arbitrary jump in a given state in ϵ.

III. STABILITY OF NORMAL ROLLS

The behavior of the system after a voltage-frequency jump depends on parameters and is related to the stability of a given initial state. A given state is obviously stable if the pattern remains unchanged and unstable if some pattern evolution drives the system away from a given initial state. In the present experiment stable normal rolls are observed at small values of ϵ and the initial wave number adequately close to k_c. In the case of unstable normal rolls, we observed two kinds of destabilization mechanisms: (i) evolutions *via* spatial modulation of the initial pattern and (ii) evolutions without any modulations.

In this section, we first give a qualitative overview of these instability processes, and then proceed to the stability diagrams obtained in the present experiments. Finally we investigate the transition scenarios for the onset of weak turbulence.

A. Pattern evolutions *via* modulational instabilities

In the first case (i), the evolution always begins with the long-wavelength modulation of the initial rolls. The modulations observed are classified into three characteristic types. In Figs. 2, 3, and 4 the typical evolutions of these three modulational instabilities are shown during the early transient away from the initial normal rolls. In order to characterize these modulational instabilities more clearly, we calculated the two-dimensional spatial power spectra from the optical images of these pattern evolutions. The power spectrum before the jump exhibits the sharp peaks at $\mathbf{k}_0$ and $2\mathbf{k}_0$, where $\mathbf{k}_0$ is the initial wave vector of the pattern. As instability evolves, new peaks exponentially develop at $\mathbf{k}_0\pm\mathbf{k}_u$ and also at the multiple combinations of $\mathbf{k}_0$ and $\mathbf{k}_u$, where $\mathbf{k}_u$ corresponds to the wave vector of the modulation. Three modulational instabilities as shown in Figs. 2, 3, and 4 can be distinguished from each other by the relative direction of the wave vector $\mathbf{k}_u$ with respect to $\mathbf{k}_0$, as is shown in Fig. 5. When $\mathbf{k}_u$ is parallel to $\mathbf{k}_0$ we call it the Eckhaus instability. When $\mathbf{k}_u$ is perpendicular to $\mathbf{k}_0$, we call it zigzag instability and otherwise the skewed varicose instability. The new peaks at $\mathbf{k}_0\pm\mathbf{k}_u$ are usually broader than the initial one at $\mathbf{k}_0$. This indicates that nearby modes around the *fastest growing* one with the wave vector $\mathbf{k}_u$ are also excited. In the present experiment the type of secondary instability was determined from the relative orientation of $\mathbf{k}_u$ together with direct observation of the pattern evolution. Aspects of these three instabilities are briefly described.

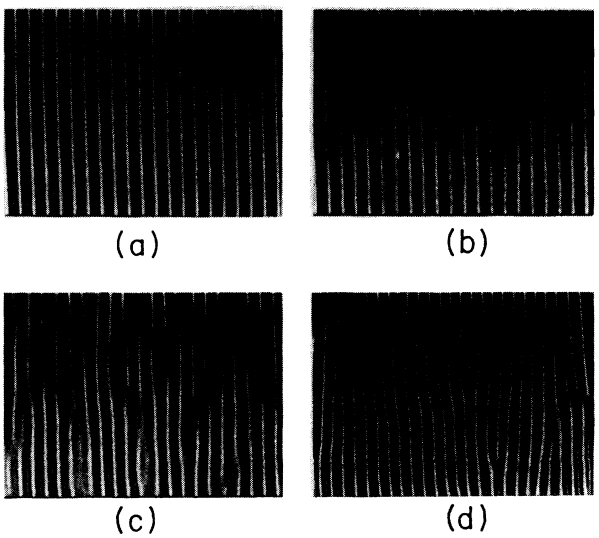

FIG. 2. Typical pattern evolution initiated by the Eckhaus instability ($k/k_c=0.83$, $\epsilon=0.12$, $f=580$ Hz). Only the early stage of the evolution is shown: (a) initial state, (b) 4.8 sec, (c) 6 sec, and (d) 7.2 sec after the voltage-frequency jump. Note that the original uniform rolls receive the compression-dilatation modulations.

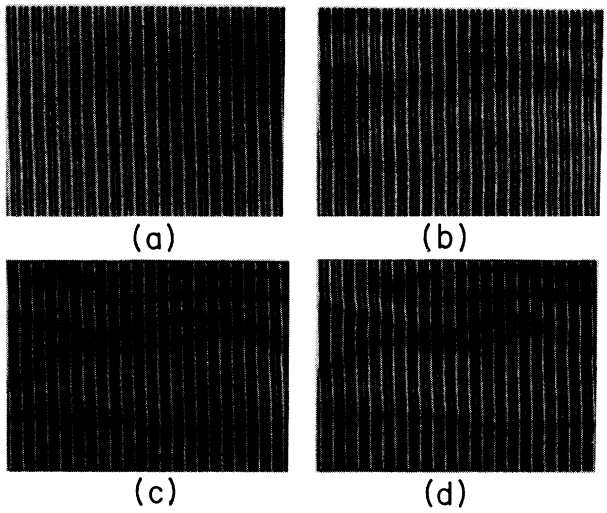

FIG. 3. Typical pattern evolution initiated by the zigzag instability ($k/k_c=1.0$, $\epsilon=0.27$, $f=400$ Hz). Only the early stage of the evolution is shown: (a) Initial state, (b) 10 sec, (c) 13.3 sec, and (d) 16.7 sec after the voltage-frequency jump. Note that the primary rolls are tilted with zigzag shape. In this case the growth of zigzag perturbation saturates at around (b) and in the subsequent stage only the quite slow dynamics of grain boundary can be seen.

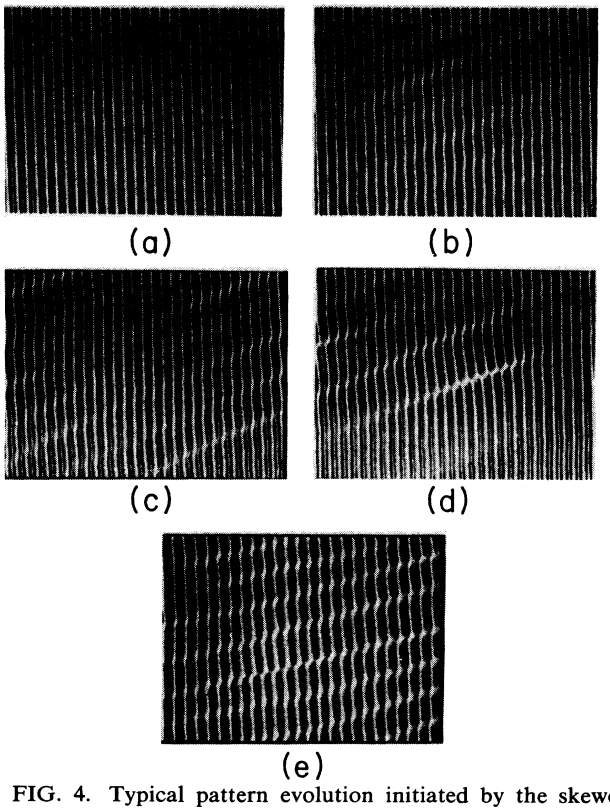

FIG. 4. Typical pattern evolution initiated by the skewed varicose instability on the normal rolls ($k/k_c=1.04$, $\epsilon=0.22$, $f=700$ Hz). Only the early stage of the evolution is shown: (a) initial state, (b) 18 sec, (c) 24 sec, and (d) 42 sec after the voltage-frequency jump. (e) The skewed varicose modulation observed in another sample under similar experimental configuration. Note that the original uniform rolls receive the periodic skew modulation.

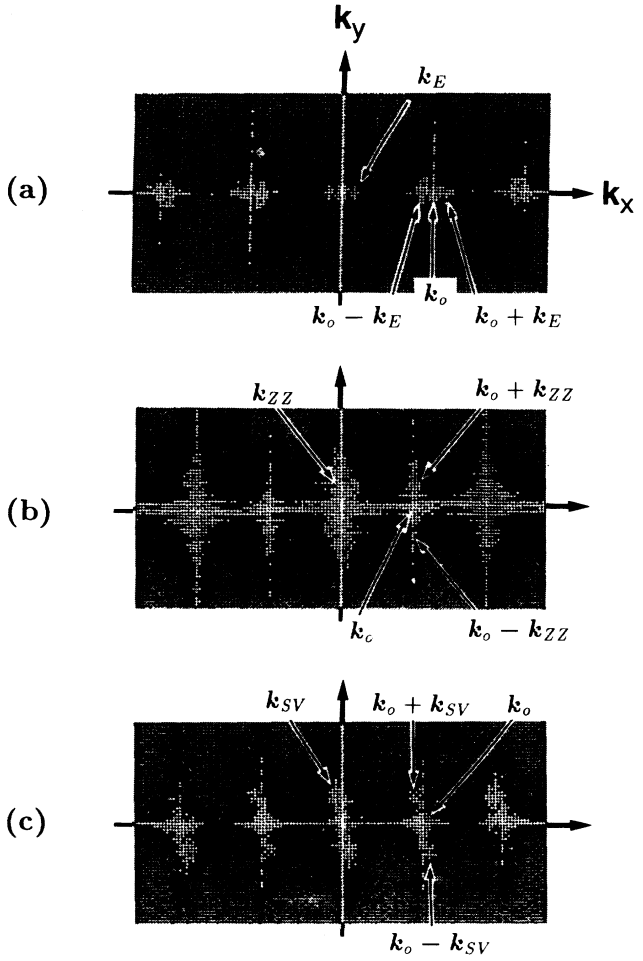

FIG. 5. Two-dimensional power spectrum obtained in the initial stage of (a) the Eckhaus instability, (b) the zigzag instability, and (c) the skewed varicose instability. The peak at $\mathbf{k}_0$ corresponds to the initial wave vector. The peaks at $\mathbf{k}_E$, $\mathbf{k}_{ZZ}$, and $\mathbf{k}_{SV}$ are responsible for the fastest-growing Eckhaus modulation, zigzag modulation, and skewed varicose modulation, respectively. The Fourier spectra images are displayed using the log operation (Ref. [22]) to enhance the low-level information.

1. Eckhaus instability

The first type of modulational instability observed here appears as a compression and dilatation of rolls along the longitudinal direction, as can be seen from Fig. 2. This instability is observed when the initial wave number is chosen adequately far from k_c. For the rolls with k smaller (larger) than k_c, this instability develops the over-compressed (over-dilated) regions in which local wavelengths are farther away from k_c than the original one. As the instability develops, the amplitudes of the flow approach zero at these over-compressed (over-dilated) regions, and eventually the elimination (nucleation) of roll pairs takes place. Figure 2 shows an example of pattern evolution in the case of $k<k_c$. The corresponding two-dimensional power spectra taken during the destabilization show the development of new peaks at

$\mathbf{k}_0 \pm \mathbf{k}_E$, where $\mathbf{k}_E$ is parallel to $\mathbf{k}_0$ [see Fig. 5(a)]. Apparently these features are a manifestation of Eckhaus instability [23]. However, in contrast to pure one-dimensional Eckhaus instability, the modulations are not homogeneous along the y direction, and thus the nucleation and elimination of roll pairs are usually accompanied with an appearance of dislocations, as is seen in Fig. 2. These observations are in agreement with others [24] and theoretical calculations [25,26].

2. *Zigzag instability*

The second type of modulational instability leads to long-wavelength zigzaglike modulations of the rolls along their axis as shown in Fig. 3. The rolls are tilted with two oblique angles $\pm\theta$ with respect to the y axis and the domains with different sign of tilt angle are separated sharply by the narrow transition regions (i.e., grain boundaries). In the two-dimensional power spectrum this instability can be characterized by the appearance of new peaks at $\mathbf{k}_0 \pm \mathbf{k}_{ZZ}$, with $\mathbf{k}_{ZZ}$ perpendicular to $\mathbf{k}_0$ [see Fig. 5(b)]. We find that in contrast to isotropic systems [2] this instability can occur for normal rolls not only for $k < k_c$ but also for $k > k_c$.

3. *Skewed varicose instability*

The third type of instability develops the periodic skew deformations of original rolls, as shown in Fig. 4. As can be seen in Fig. 4, the bending distortion due to this instability is not smooth but localized over one or two roll distances along the y direction, causing shear displacement of rolls there. As the instability develops, this shear displacement of rolls increases, and eventually the pinching of the rolls and the nucleation of defect pairs take place at several points along the shear lines. In general two symmetrical skew deformations develop simultaneously in different areas of the sample. The corresponding power spectra taken during the destabilization show the appearance of new peaks at $\mathbf{k}_0 \pm \mathbf{k}_{SV}$, where $\mathbf{k}_{SV}$ is oblique to $\mathbf{k}_0$ [see Fig. 5(c)].

B. Pattern evolutions without modulational instabilities

In the second case (ii), the pattern evolution is much simpler than those described above. Immediately after the voltage-frequency jump, the initial pattern begins to decay exponentially without any deformation. After the jump to $\epsilon < 0$, the resulting state is always the homogeneous state without convection. On the other hand, for $\epsilon > 0$, a new normal-roll pattern with a wave number close to k_c appears after the exponential decay of the initial pattern. This kind of pattern evolution is known to occur in the parameter region below the neutral stability curve for the onset of convection, where the primary mode has a negative linear growth rate [14,27].

C. Stability diagrams

The quantitative results for the stability of normal rolls are summarized in Fig. 6, in which the stability of normal rolls is shown in the (q,ϵ) plane for three values of the external frequency f. The symbols represent the experimentally determined stability of normal rolls: The closed circle indicates stable normal rolls, and the open circle, the open square, and the open diamond, respectively, indicate the location where the Eckhaus, the zigzag, and the skewed varicose (SV) instabilities are observed as the

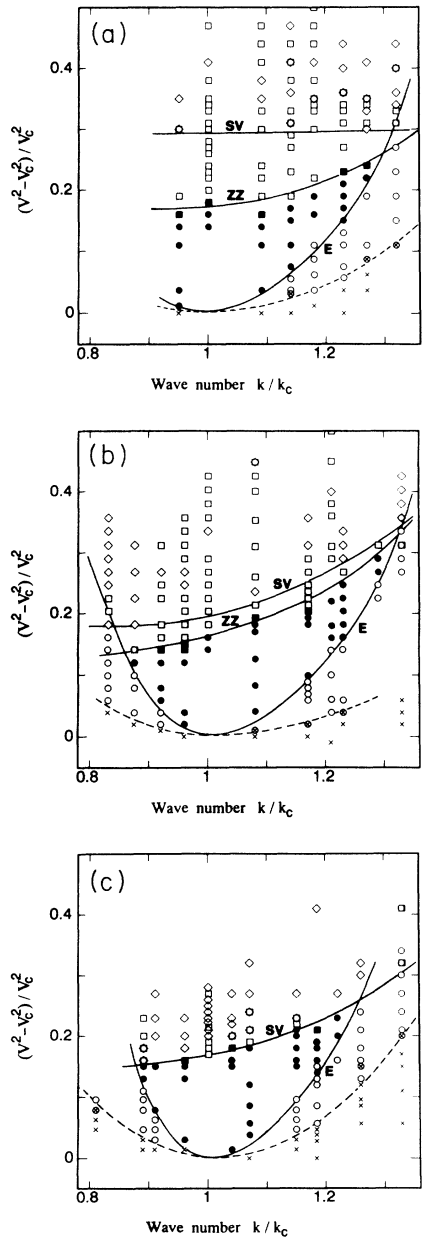

FIG. 6. The stability of normal rolls as a function of the reduced voltage $\epsilon = (V^2 - V_c^2)/V_c^2$ and the reduced wave number k/k_c is plotted for three frequencies (a) 400 Hz, (b) 580 Hz, and (c) 700 Hz. Symbols represent experimental data points and the lines are guides to the eye. Closed circles refer to linearly stable and crosses refer to absolutely decaying normal rolls. Open circles, open squares, and open diamonds refer to the locations where the normal rolls become unstable against Eckhaus, zigzag, and skewed varicose instabilities, respectively.

fastest-growing one. The cross indicates absolutely unstable normal rolls, i.e., where the initial mode decays exponentially without deformations. Based on these experimental points given in Fig. 6 we divide the (q,ϵ) space into several regions by smooth curves as guides to the eye. In Fig. 6(a) we have only a few data points for $k < k_c$, because smaller values of k cannot be achieved by the voltage-frequency jumping method [see Fig. 1(b)].

As can be seen in Fig. 6, for all frequencies measured in the present experiments the Eckhaus instability dominates in the lower part of the stability diagrams, i.e., the stable bands of the normal rolls are bounded by the Eckhaus instability for small values of ϵ. However the instability that dominates in the upper part of the stability diagrams strongly depends on the frequency.

At the low frequency $f=400$ Hz, near the upper boundary of the stable region the zigzag instability is dominant, as can be seen in Fig. 6(a). We always observed the zigzag-type instability in the region in between the ZZ curve and the SV curve. On the other hand, above the SV curve the most rapidly growing mode is either the zigzag or the skewed varicose instability, and it is in addition not fully reproducible whether the modulational instability corresponds to the zigzag or the skewed varicose. Moreover after a voltage-frequency jump above the SV curve, we sometimes observed complicated competition between these modes during the transient away from the initial normal rolls. These indicate that above the SV curve both the zigzag and the skewed varicose mode have a positive growth rate. The y component of the wave vector of the fastest-growing zigzag mode tends to decrease as an initial state approaches the ZZ curve from above. At the higher frequency $f=580$ Hz [Fig. 6(b)], the region where the skewed-varicose-type instability takes place is shifted to lower values of ϵ than that at $f=400$ Hz. However, the zigzag instability is still dominant in the narrow region immediately above the top boundary of the stable region for normal rolls.

At the frequency $f=700$ Hz [Fig. 6(c)], the zigzag instability seems to be no longer dominant in the upper part of the stability diagram. We observed the skewed varicose instability already immediately above the top boundary of the stable region for normal rolls. As the initial state approaches the SV curve from above, both x and y components of the wave vector $\mathbf{k}_u$ of the skewed varicose mode decrease and seem to vanish at the SV curve. However it is difficult to make the quantitative determination on the wave vector $\mathbf{k}_u$ at this frequency, because the corresponding peaks in the Fourier spectra measured during the early stage of the destabilization are broader than at 400 Hz and 580 Hz. In addition the maxima of the new peaks become weaker in the region close to the SV curve. This is also the origin of the difficulty in deciding whether the observed instability is of the zigzag type or of the skewed varicose type, especially in the region close to the SV curve. Therefore, within the errors, it is possible that the open squares close to the SV curve in Fig. 6(c) also correspond to the skewed varicose instability. Moreover, even when the fastest-growing mode is judged as the zigzag type by our criterion, we usually observed the skewed-varicose-type roll deformations in the subsequent stage of the pattern evolution. Hence the dominant instability above the upper boundary of the stable region is most likely of the skewed varicose type at this frequency.

D. Routes to weak turbulence

Here we describe the routes to weak turbulence in this system in conjuction with the stability diagrams shown in Fig. 6. As described above the most effective secondary instability at increasing ϵ is the zigzag instability for low frequencies and the skewed varicose instability for high frequencies. One may, therefore, expect in the respective frequency ranges different transition scenarios from the normal rolls to the weak turbulent state (FWR). To verify this we increased at various frequencies the voltage by small steps of 0.05 V with long enough intervals between every step. The results are summarized in Fig. 7, in which qualitatively different scenarios can be seen depending on the frequency.

For the low-f-regime, where the destabilizing mechanism at the second bifurcation is expected to be the zigzag instability, the following sequence of bifurcations was observed. (1) The first bifurcation from the rest state to the stationary normal rolls takes place at $\epsilon=0$. (2) Increasing the voltage further the second bifurcation from the normal rolls to the zigzag rolls [Fig. 8(b)] takes place at second thresholds ϵ_s. (3) At some critical values ϵ_t the third bifurcation from the zigzag rolls to the FWR with sustained irregular defect motion [Fig. 8(d)] occurs. At $f=400$ Hz, where we obtained our stability diagram shown in Fig. 6(a), we find $\epsilon_s=0.17\pm0.02$ and $\epsilon_t=0.35\pm0.02$. In the zigzag-roll regime the tilt angle of the rolls with respect to the y axis increases with the deviation $\epsilon-\epsilon_s$ from the second threshold for a given frequency. We found also that the maximum tilt angle θ_m just below the third threshold ϵ_t decrease with increasing f.

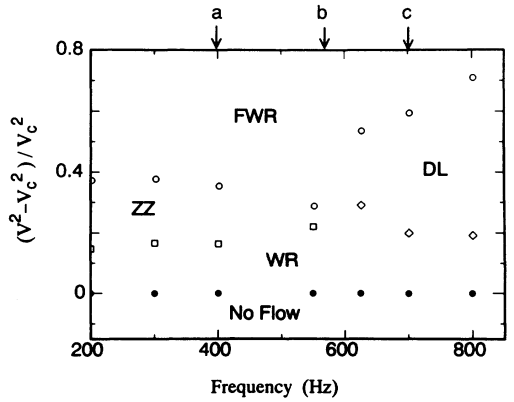

FIG. 7. Phase diagram for EHC obtained by increasing the voltage at each frequency. WR, ZZ, DL, and FWR represent normal rolls (Williams rolls), zigzag pattern, defects lattice, defect turbulence (fluctuating Williams rolls) phase, respectively. Symbols indicate the critical points at which a transition between different phases are observed by increasing the voltage. Arrows denote the frequencies at which the stability diagrams in Fig. 6 are obtained. See also Fig. 8.

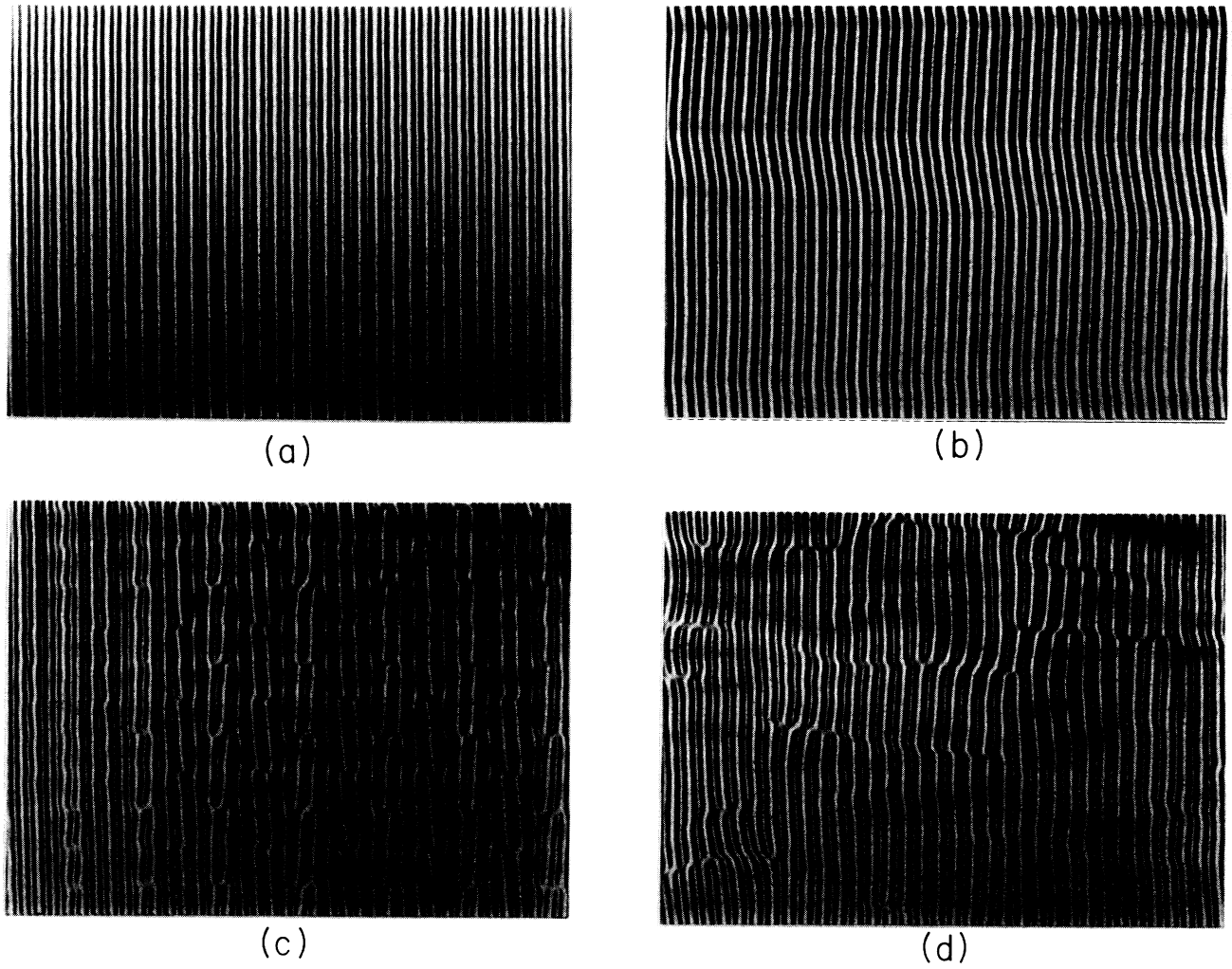

FIG. 8. Optical images of four typical patterns in EHC: (a) Normal rolls (WR's), (b) zigzag rolls (ZZ), (c) defect lattice structure (DL), and (d) fluctuating Williams rolls (FWR's).

At higher frequencies, where the dominant destabilization mechanism at the second bifurcation was of the skewed varicose type (see Fig. 6), the observed sequence of the bifurcation is as follows. (i) The first bifurcation to the stationary normal-rolls state takes place at $\epsilon=0$. (ii) At the second threshold ϵ_s, the normal rolls become unstable. However the secondary pattern after the bifurcation is not the zigzag pattern but instead a new convective pattern in which the bounded defect pairs form a two-dimensional lattice structure as is shown in Fig. 8(c). The distances of these defect pairs in both the x and y direction tend to diverge near ϵ_s and decreases with an increase in ϵ. Each defect pair shown in Fig. 8(c) oscillates at each lattice site. The characteristic frequency of this oscillation increases with $\epsilon-\epsilon_s$ [28]. We refer to this new convective state as a defect lattice. A similar pattern was also observed in Refs. [18 and 29], whereas in Ref. [29] the experiments were performed with pure MBBA. (iii) At the third threshold ϵ_t, the defect lattice becomes unstable and changes into a FWR. At the present moment, however, it is not clear whether the nature of the FWR in this frequency regime is the same as that in the lower frequency regime. At $f=700$ Hz, where we got the stability diagram shown in Fig. 6(c), we find $\epsilon_s=0.20\pm0.02$ and $\epsilon_t=0.59\pm0.02$.

A transfer from the first scenario to the second one occurs in the frequency range $550<f<620$ Hz, where the stability diagram shown in Fig. 6(b) is obtained. As can be seen in Fig. 7 the distance between ϵ_s and ϵ_t for a given frequency decreases as the operating frequency is closer to this crossover-frequency regime. Therefore it becomes difficult to identify in the crossover regime the secondary ordered state between the WR phase and the FWR phase. This leads us to the third scenario with the direct transition from a WR to a FWR.

In the normal-rolls regime the pattern remains perfectly periodic, but its wave number k tends to increase approximately as $k=a\epsilon+k_c$, where $a=0.15\pm0.05$ for the frequencies displayed in Fig. 7. Extrapolating this to Fig. 6 the second bifurcation point could be predicted at $\epsilon_s=0.17\pm0.01$ for $f=400$ Hz and at $\epsilon_s=0.17\pm0.01$ for $f=700$ Hz, because the selected wave number should

cross the instability boundary at these values of ϵ. These thresholds agree with the measured values within experimental errors.

IV. DISCUSSION AND CONCLUSION

We have measured the stability of normal-oriented rolls in EHC and found that there exist three destabilizing modes, i.e., the Eckhaus, the zigzag, and the skewed varicose instability. All three instabilities are also relevant for the stability of straight convection rolls in Rayleigh-Bénard convection in simple isotropic fluids [2]. In isotropic systems the zigzag instability always takes place for $k < k_c$ and is understood as a wavelength adjusting mechanism for straight convection rolls, because the length of the effective wave vector always gets closer to k_c through the zigzag deformation. In EHC the zigzag instability occurs also for $k > k_c$ as is shown in Fig. 6 and triggers the transition from a normal-rolls to a zigzaglike pattern. Therefore in EHC the zigzag instability acts more like a wave-vector-adjusting mechanism. In isotropic systems the skewed varicose instability plays an essential role in the transition to weak turbulence [10]. On the other hand, in EHC the skewed varicose instability generally leads to a new ordered pattern, i.e, the zigzag pattern at low frequencies and the defect lattice at high frequencies.

Recent analysis of the stability of normal rolls qualitatively agrees with the present results [12,13,25,30]. The calculations were done on two-dimensional anisotropic model systems [12,25] and directly in the framework of the electrohydrodynamic equations [13,30]. In both works special attention was paid to the mean-flow effects. These calculations show that the zigzag instability and the skewed varicose instability are dominant in the upper part of the stability diagram. However there seems up to now no quantitative agreement between the experimental and the theoretical results. The lack of the quantitative agreement is perhaps related to different material constants used in calculations, to the incompleteness of the fundamental equations and boundary effects at the electrodes [31].

We have here only considered the stability of the normal rolls. The stability of the oblique rolls remains an interesting problem, because the differences between EHC and RBC should be more drastic. It was shown, e.g., in Ref. [32] that the oblique rolls are destabilized by the skewed-varicose-like instability, which leads to a stationary ordered pattern, i.e., the so-called varicose pattern. Another interesting question related to the difference between isotropic and anisotropic systems would be to measure also the k_y dependence of the neutral stability $[V_0(k_{xc},k_y,f)]$ and to compare it with the theoretical predictions about a neutral surface for EHC [27,33].

In the present experiment three different transition scenarios from the straight convection rolls to weak turbulence have been observed in the identical sample: (i) the WR-zigzag-FWR, (ii) the WR-FWR, and (iii) the WR-(defect-lattice)-FWR. The selection of these scenarios strongly depends on the external frequency f. According to the stability diagram obtained in the present experiments, such a change in the scenario with f seems to be closely related to the change of the destabilizing mechanism at the second threshold.

Recently in the first scenario of a WR-zigzag-FWR another group made similar investigations [16]. In this work several samples with several cell thicknesses and several aspect ratios have been investigated in a restricted range of the external frequency. They concluded from their measurements that there is some maximum tilt angle of the zigzag rolls for the onset of the persistent nucleation and annihilation of defects (FWR). However the present results will not support them. We find that the maximum tilt angle at the transition threshold ϵ_t to a FWR changes as a function of the frequency of the external voltage and goes presumably to zero at some medium frequency. In a previous study [15], we observed the second scenario of a WR-FWR. At that time we found that the skewed varicose boundary locates just above the zigzag boundary. This qualitatively agrees with the present results. However the physical origin of the direct transition from a WR to a FWR remains unresolved. On the transition scenario WR-(defect-lattice)-FWR, a number of interesting questions clearly remain unresolved. In particular, the formation mechanism and the quantitative characterization of a defect lattice pattern are subjects of further investigation [28].

ACKNOWLEDGMENTS

We would like to thank H. R. Brand, W. Pesch, S. Sasa, and M. Sano for discussions. W. Z. is grateful to the Kyushu Institute of Technology (KIT) for a stay during which this cooperation was started and to the Kajima Foundation which made a second stay at the KIT and Kyushi University possible. This work was partially supported by the Grant-in-Aid for Scientific Research from the Ministry of Education, Science and Culture of Japan.

[1] For numerous examples and references, see for instance, *Cellular Structures in Instabilities,* edited by J. E. Wesfreid and S. Zaleski (Springer, New York, 1984); *Propagation in Systems Far from Equilibrium,* edited by J. E. Wesfreid *et al.* (Springer, Berlin, 1988); *Nonlinear Evolutions of Spatio-Temporal Structures in Dissipative Continuous Systems,* edited by F. H. Busse and L. Kramer (Plenum, New York, 1990); P. C. Hohenberg and J. S. Langer, J. Stat. Phys. **28**, 193 (1982).

[2] F. H. Busse, Rep. Prog. Phys. **41**, 1929 (1978); in *Hydrodynamic Instabilities and the Transition to Turbulence,* edited by H. L. Swinney and J. P. Gollub (Springer, Berlin, 1981).

[3] L. M. Blinov, *Electro-Optical and Magneto-Optical Proper-*

ties of Liquid Crystals (Wiley, New York, 1983).
[4] S. Kai and W. Zimmermann, Prog. Theor. Phys. **99**, 458 (1989).
[5] For a recent review see W. Zimmermann, MRS Bull. **XVI**, 46 (1991).
[6] P. C. Hohenberg and B. I. Shraiman, Physica D **37**, 109 (1989).
[7] Y. Kuramoto, Prog. Theor. Phys. Suppl. **64**, 346 (1978); *Chemical Oscillations, Waves and Turbulence* (Springer, Berlin, 1984).
[8] H. Chaté and P. Manneville, Phys. Rev. Lett. **58**, 112 (1987); see also K. Kaneko, Prog. Theor. Phys. **74**, 1033 (1985).
[9] P. Coullet, L. Gil, and J. Lega, Phys. Rev. Lett. **62**, 1619 (1989).
[10] A. Pocheau, V. Croquette, and P. Le Gal, Phys. Rev. Lett. **55**, 1094 (1985).
[11] M. S. Heutmaker and J. P. Gollub, Phys. Rev. A **35**, 242 (1987).
[12] S. Sasa, Prog. Theor. Phys. **83**, 824 (1990).
[13] M. Kaiser, W. Pesch, and E. Bodenshatz (unpublished).
[14] M. Lowe and J. P. Gollub, Phys. Rev. Lett. **55**, 2575 (1985).
[15] S. Nasuno and S. Kai, Europhys. Lett. **14**, 779 (1991).
[16] E. Braun, S. Rasenat, and V. Steinberg, Europhys. Lett. **15**, 597 (1991).
[17] K. Hirakawa and S. Kai, Mol. Cryst. Liq. Cryst. **40**, 261 (1977); S. Kai and K. Hirakawa, Prog. Theor. Phys. Suppl. **64**, 212 (1978).
[18] S. Nasuno, Ph.D. thesis, Tohoku University, 1990 (in Japanese).
[19] R. Ribotta, A. Joets, and Lin Lei, Phys. Rev. Lett. **56**, 1595 (1986).
[20] S. Kai, N. Chizumi, and M. Kohno, J. Phys. Soc. Jpn. **58**, 1493 (1989); Phys. Rev. A **40**, 6554 (1990).
[21] G. Goren, I. Procaccia, S. Rasenat, and V. Steinberg, Phys. Rev. Lett. **63**, 1237 (1989).
[22] R. G. Gonzalez and P. Wintz, *Digital Image Processing*, 2nd ed. (Addison-Wesley, Reading, MA, 1987).
[23] W. Eckhaus, *Studies in Nonlinear Stability Theory* (Springer, Berlin, 1965).
[24] S. Rasenat, E. Braun, and V. Steinberg, Phys. Rev. A **43**, 5728 (1991).
[25] E. Bodenschatz, M. Kaiser, L. Kramer, W. Pesh, A. Weber, and W. Zimmermann, in *New Trends in Nonlinear Dynamics and Pattern-Forming Phenomena*, Vol. 237 of *NATO Advanced Study Institute, Series B: Physics*, edited by P. Coullet and P. Huerre (Plenum, New York, 1991).
[26] L. Kramer and W. Zimmermann, Physica D **16**, 221 (1985); L. Kramer, H. Schober, and W. Zimmermann, *ibid.* **31**, 212 (1988).
[27] E. Bodenschatz, W. Zimmermann, and L. Kramer, J. Phys. (Paris) **49**, 1875 (1988).
[28] S. Nasuno *et al.* (unpublished).
[29] H. Yamazaki, S. Kai, and K. Hirakawa, J. Phys. Soc. Jpn. **52**, 1878 (1983).
[30] W. Pesch (unpublished).
[31] W. Zimmermann, in *Defects, Singularities and Patterns in Nematic Liquid Crystals, NATO Advanced Study Institute Series*, edited by J. M. Coron, F. Helen, and J. M. Ghidaglia (Kluwer, Dordrecht, 1991); H. R. Brand and H. Pleiner, Phys. Rev. A **35**, 3122 (1987); W. Zimmermann, H. R. Brand, and H. Pleiner (unpublished).
[32] A. Joets and R. Ribotta, J. Phys. (Paris) **47**, 595 (1986); **47**, 739 (1986).
[33] W. Zimmermann and L. Kramer, Phys. Rev. Lett. **55**, 402 (1985).

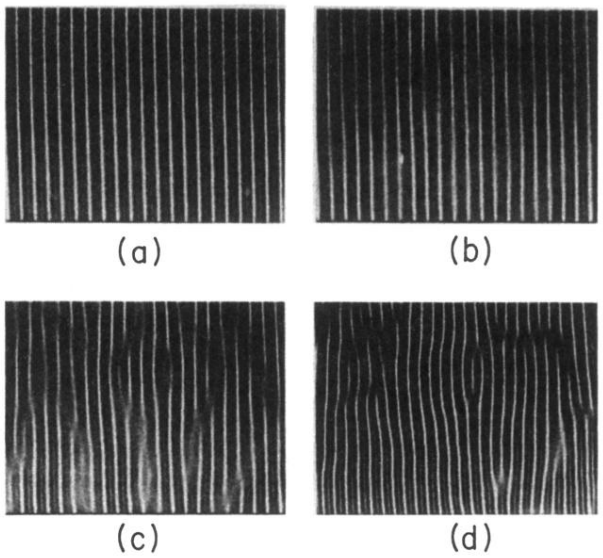

FIG. 2. Typical pattern evolution initiated by the Eckhaus instability ($k/k_c=0.83$, $\epsilon=0.12$, $f=580$ Hz). Only the early stage of the evolution is shown: (a) initial state, (b) 4.8 sec, (c) 6 sec, and (d) 7.2 sec after the voltage-frequency jump. Note that the original uniform rolls receive the compression-dilatation modulations.

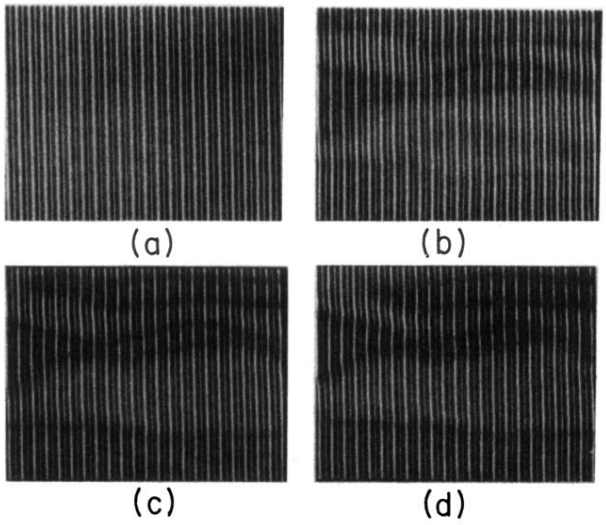

FIG. 3. Typical pattern evolution initiated by the zigzag instability ($k/k_c = 1.0$, $\epsilon = 0.27$, $f = 400$ Hz). Only the early stage of the evolution is shown: (a) Initial state, (b) 10 sec, (c) 13.3 sec, and (d) 16.7 sec after the voltage-frequency jump. Note that the primary rolls are tilted with zigzag shape. In this case the growth of zigzag perturbation saturates at around (b) and in the subsequent stage only the quite slow dynamics of grain boundary can be seen.

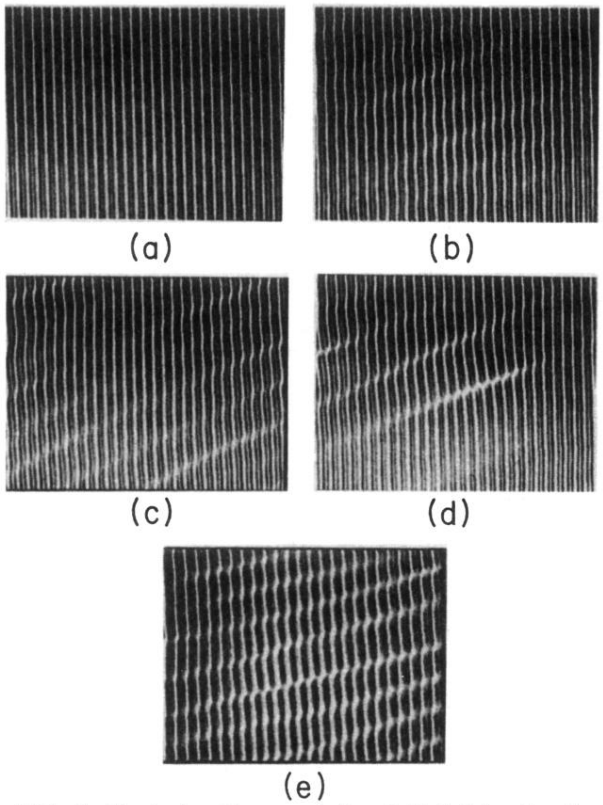

FIG. 4. Typical pattern evolution initiated by the skewed varicose instability on the normal rolls ($k/k_c=1.04$, $\epsilon=0.22$, $f=700$ Hz). Only the early stage of the evolution is shown: (a) initial state, (b) 18 sec, (c) 24 sec, and (d) 42 sec after the voltage-frequency jump. (e) The skewed varicose modulation observed in another sample under similar experimental configuration. Note that the original uniform rolls receive the periodic skew modulation.

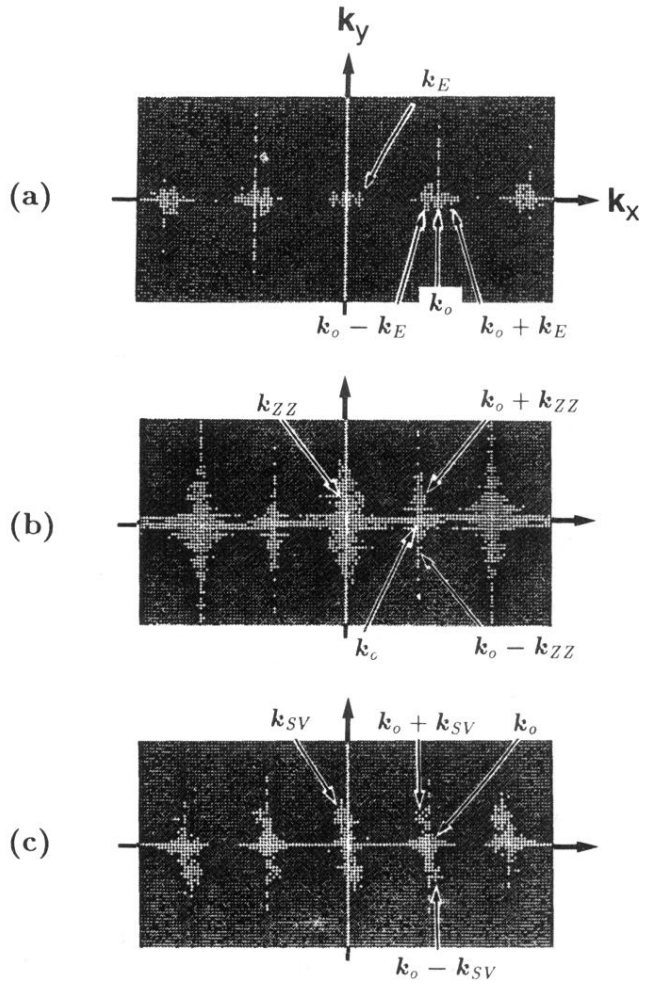

FIG. 5. Two-dimensional power spectrum obtained in the initial stage of (a) the Eckhaus instability, (b) the zigzag instability, and (c) the skewed varicose instability. The peak at $\mathbf{k}_0$ corresponds to the initial wave vector. The peaks at $\mathbf{k}_E$, $\mathbf{k}_{ZZ}$, and $\mathbf{k}_{SV}$ are responsible for the fastest-growing Eckhaus modulation, zigzag modulation, and skewed varicose modulation, respectively. The Fourier spectra images are displayed using the log operation (Ref. [22]) to enhance the low-level information.

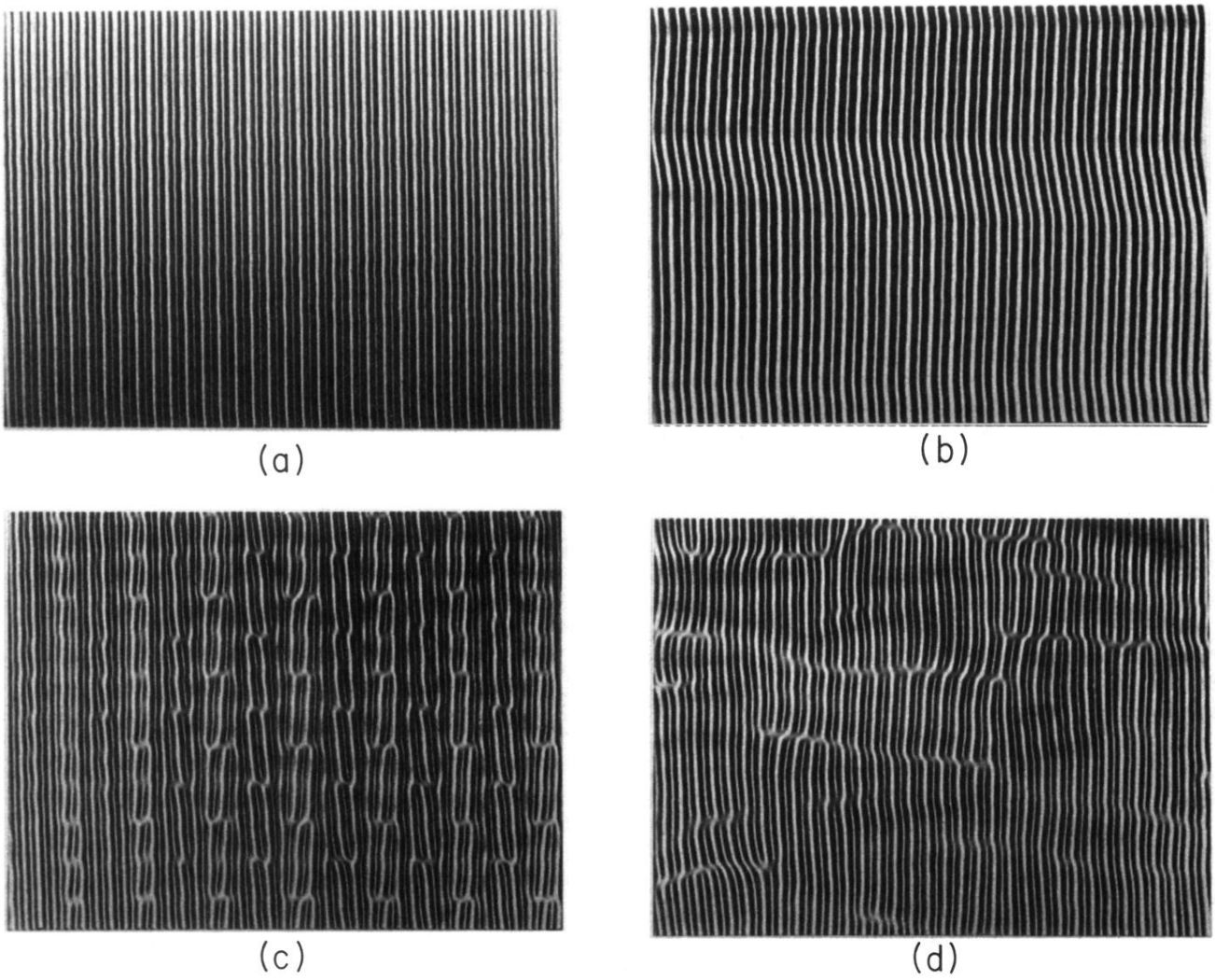

FIG. 8. Optical images of four typical patterns in EHC: (a) Normal rolls (WR's), (b) zigzag rolls (ZZ), (c) defect lattice structure (DL), and (d) fluctuating Williams rolls (FWR's).